Detection and Characterization of Individual Intermolecular Bonds Using Optical Tweezers

Andrea L. Stout
Department of Physics and Astronomy, Swarthmore College, Swarthmore, Pennsylvania 19081 USA

ABSTRACT The development of scanning probe techniques has made it possible to examine protein-protein interactions at the level of individual molecular pairs. A calibrated optical tweezers, along with immunoglobulin G (IgG)-coated polystyrene microspheres, has been used to detect individual surface-linked *Staphylococcus* protein A (SpA) molecules and to characterize the strength of the noncovalent IgG-SpA bond. Microspheres containing, on average, less than one IgG per contact area were held in the optical trap while an SpA-coated substrate was scanned beneath them at a distance of ~50 nm. This geometry allows the trapped bead to make contact with the surface, from bond formation to rupture, and results in an enhancement of the force applied to a bond due to leverage supplied by the bead itself. Experiments yielded median single-bond rupture forces from 25 to 44 pN for IgG from four mammalian species, in general agreement with predictions based on free energies of association obtained from solution equilibrium constants.

INTRODUCTION

Specific bimolecular interactions are central to virtually all biological processes. Until recently, most investigations of such interactions have been performed under equilibrium conditions with the reactants free in solution, unperturbed by any net external force. Data gathered under such conditions have enabled the determination of a vast array of equilibrium and kinetic constants for various molecular pairs. For some molecules, however, the environment of the solution binding study is not an accurate reproduction of conditions that are relevant in vivo. In particular, phenomena such as cell-surface and cell-cell adhesion as well as muscle fiber contraction often occur in the presence of external loads, with reactants far from equilibrium. Experiments using flow fields to apply external loads to adherent cells have supported predictions that stress can strongly influence the equilibrium and kinetics of intermolecular interactions (Pierres et al., 1995; Alon et al., 1995; Kuo and Lauffenburger, 1993). With the advent of probe microscopy techniques, examination of the interactions between individual molecular pairs has become possible. Rupture forces between molecular pairs have been measured by atomic force microscopy (Ros et al., 1998; Hinterdorfer et al., 1996; Florin et al., 1994), optical tweezers (Helmerson et al., 1997; Nishizaka et al., 1995), and micropipette-aspirated vesicles (Evans et al., 1991). Reported in this paper are the results of experiments designed to detect individual protein-protein interactions and measure the forces required to rupture them.

To explore the influence of applied forces on the dynamics of individual protein-protein bonds, a scanning optical force microscope based on that of Ghislain et al. (1994), in which an optical tweezers functions as a force transducer, was constructed. Optical tweezers have been used to measure the piconewton forces generated by single motor molecules such as kinesin and myosin (Finer et al., 1994; Svoboda et al., 1993) as well as by individual molecules of RNA polymerase (Yin et al., 1995). They are generally considered effective force transducers in the range spanning 0.5 to 50 pN, the upper limit depending primarily on available laser power and the size of the probe particle. By exploiting the interaction between probe and surface, it is possible to obtain an approximately fivefold enhancement of the force applied by the optical tweezers. Fig. 1 is a cartoon depicting the general experimental scheme. A probe particle coated with a small number of ligand molecules is held in the stationary optical trap while a flat substrate, sparsely coated with receptors, is scanned beneath it. Lateral displacements of the probe away from its equilibrium position in the trap are monitored during the scan with an *x*-*y* position detector. Binding events between the trapped probe and the moving substrate result in displacement signals with a characteristic shape. Once bound, the probe moves with the substrate until the force applied by the optical tweezers overcomes the bond. Bond rupture allows the restoring force of the optical trap to rapidly pull the probe back to the trap center. Enhancement of the applied force comes about when, before bond breakage, the probe particle becomes pinned against the substrate, acting as a lever (Sagvolden, 1999; Chang and Hammer, 1996). This leverage can potentially allow the optical tweezers to access rupture forces in the 100–200-pN range, which would otherwise be inaccessible.

This paper reports on a study of the interaction between protein A from *Staphylococcus aureus* (SpA) and immunoglobulin G (IgG) from four mammalian species. SpA is a bacterial Fc receptor frequently used in immunological applications (for a review, see Langone, 1982). Measurements of the forces required to detach IgG-coated beads from SpA-coated surfaces have been carried out using flow fields

Received for publication 18 May 2000 and in final form 3 March 2001.
Address reprint requests to Dr. Andrea L. Stout, Department of Physics and Astronomy, Swarthmore College, Swarthmore, PA 19081. Tel.: 610-328-8386; Fax:610-328-7895; E-mail: astout1@swarthmore.edu.

0006-3495/01/06/2976/11 $2.00

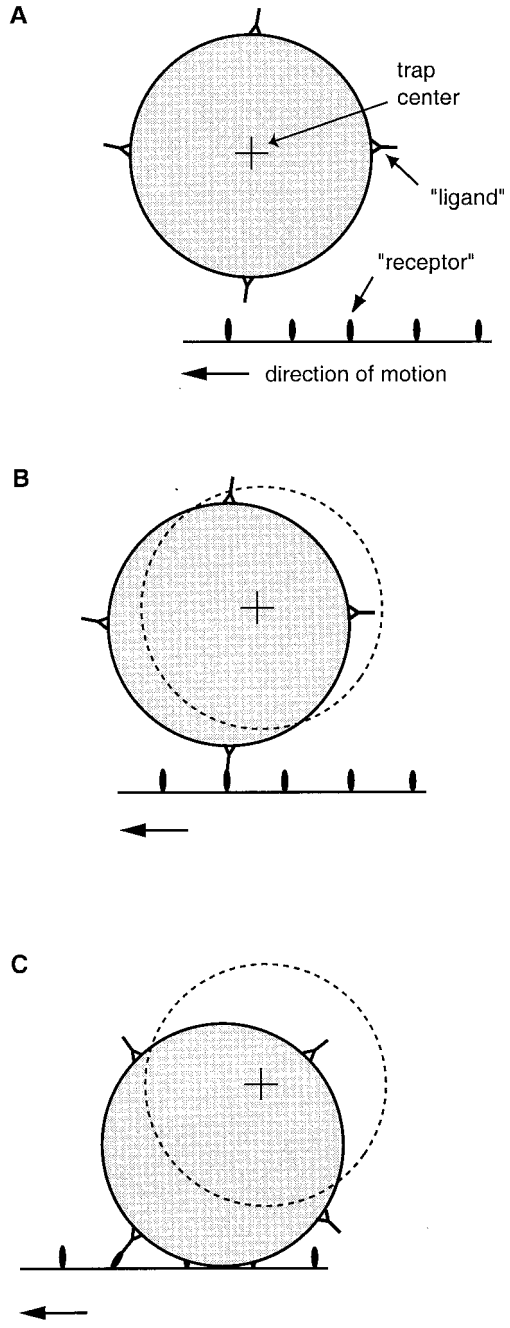

FIGURE 1 Cartoon depicting the experimental procedure. Note that this drawing is not to scale; in reality, the bead diameter is ~100 times larger than the molecular dimensions. (*A*) A bead containing a small number of "ligand" molecules is held a short distance above a moving substrate coated with "receptor" molecules. When not bound to the substrate, the bead is free to undergo Brownian motion around the center of the optical trap (+). The time-averaged force on the bead is zero under these conditions. (*B*) If the bead binds to a surface-bound receptor, it will begin to move away from its equilibrium position (represented by the ddashed circle) with the same velocity as the moving surface. As it does so, it will experience an increasing force in the direction of the trap center. (*C*) As the bead is moved further from the trap center by the substrate, it pivots and makes contact with the surface, resulting in an additional normal force. When the total force applied to the bead by the trap and the surface is sufficient to overcome the adhesion due to the receptor-ligand interaction, the bond breaks, and the bead returns to the condition shown in *A*.

(Kuo and Lauffenburger, 1993). Recently, Simson et al. (1999) used a micropipette force transducer to investigate the loading-rate dependence of the rupture force for rabbit IgG-SpA bonds. The focus of the present work is to compare single-bond rupture forces for similar bonds with different affinities.

MATERIALS AND METHODS

Sample preparation

Carboxylate-modified polystyrene (PS) microspheres were purchased from Interfacial Dynamics Corp. (Portland, OR; 1.03-μm-diameter beads) and from Bangs Laboratories (Fishers, IN; 2.6-μm-diameter beads). Unlabeled IgG and SpA were purchased from Sigma (St. Louis, MO), as were bovine serum albumin (BSA), κ-casein and 3-mercaptopropyltrimethoxysilane (MTS). Fluorescein isothiocyanate (FITC)-labeled protein A was obtained from Zymed (South San Francisco, CA). *N*-γ-maleimidobutyryloxy succinimidyl ester (GMBS) and 1-ethyl-3- (3-dimethylaminopropyl) carbodiimide were purchased from Fluka (Buchs, Switzerland).

IgG was covalently linked to microspheres according to the two-step protocol supplied by Bangs. Briefly, beads were washed three times in deionized water and then resuspended in 0.01 M K_2HPO_4, pH 4.5. Carbodiimide in water was added to yield a final concentration of 1.0% (w/v), and the beads were incubated at room temperature for 3.5 h. They were then washed and resuspended in 0.2 M sodium borate, pH 8.5, to remove unreacted carbodiimide. Purified IgG from rabbit (R-IgG), mouse (M-IgG), bovine (B-IgG), or goat (G-IgG) serum was added at a ratio of 10 protein molecules per bead for force experiments, and the mixture was allowed to sit on a rotary mixer overnight at room temperature. The next morning, ethanolamine was added to give a final concentration of 5.0 mM. After 30 min, the beads were washed several times in 0.1 M glycine, pH 8.2, 0.05% Tween 20 and resuspended in this buffer for storage at 4°C until use. IgG beads were used within 3 weeks after preparation.

SpA was coupled to glass coverslips using the procedure of Bhatia et al. (1989). The 25-mm-diameter coverslips (0.17 mm thickness) were sonicated in PEX detergent (Peck's Products, St. Louis, MO) for 20 min and then rinsed extensively with deionized water. They were then soaked in 3.0 M KOH for 1 h, rinsed extensively with deionized water, soaked in 50% H_2SO_4 for 1 h, and again rinsed with deionized water. The coverslips were dried in a 60°C oven for several hours or overnight. Coverslips were silanized in 2% solution of MTS in dry toluene for 2 h under an argon atmosphere and then rinsed in dry toluene and allowed to air dry. Next they were allowed to sit under a 2 mM solution of GMBS in 100% ethanol for 1 h. Coverslips were rinsed first in 95% ethanol and then in deionized water. Finally, 300 μl of 0.005 mg/ml SpA in phosphate-buffered saline (PBS), pH 7.4, was placed on each coverslip for 1 h. For control experiments, coverslips sat under 0.1 M ethanolamine or 1 mg/ml BSA. Coverslips were rinsed with sterile PBS and stored under the same containing 0.2% sodium azide at 4°C until use within 3 days of preparation.

Samples were prepared for force experiments in the following manner. Beads were diluted in deionized water and sonicated for 15–20 min in a bath sonicator. They were then spun down and resuspended in PBS with 80 μg/ml κ-casein. Two strips of Parafilm (Neenah, WI), 0.125 mm thick, were placed on a prepared coverslip as spacers. A 75-μl volume of bead suspension was placed on the coverslip, covered with a clean 18-mm-diameter coverslip, and the sandwich was then sealed with paraffin.

Surface density of protein

The surface density of SpA obtained using the above coating procedure was evaluated using a laser scanning confocal microscope (MRC-600 scanning box (BioRad, Hercules, CA) and an Axiovert 35 microscope

(Carl Zeiss. Thornwood, NY)) with a 60× oil immersion objective. Coverslips were coated with FITC-labeled SpA (dye:protein ratio = 3.2:1 as specified by the supplier) at three dilutions: 0.005, 0.05, and 0.1 mg/ml. Fluorescence images were obtained of these surfaces as well as of surfaces coated with unlabeled SpA. Average pixel intensities after background subtraction were compared with those for images of known concentrations of FITC in PBS (pH = 7.4) Given the known detection volume per pixel (as determined by the confocal aperture), the pixel intensity corresponding to a known number of FITC molecules could be determined. These measurements indicated that the coating procedure using 0.005 mg/ml SpA yielded a surface density of 700 SpA molecules per μm^2, or roughly 3% coverage of the surface (assuming an SpA molecule to be a prolate ellipsoid ~16 nm long and 2.3 nm wide (Langone, 1982).

Experimental apparatus

The optical tweezers apparatus is shown in Fig. 2. The TEM_{00} beam (λ = 1064 nm) from a diode-pumped Nd:YAG laser (Spectra-Physics, Mountain View, CA) was expanded to a diameter of 17 mm and directed into the bottom camera port of a custom-modified Carl Zeiss Axiovert 135 TV inverted microscope. This degree of beam expansion overfilled the back aperture of a 1.4 N.A., 63× objective (Zeiss Plan-apochromat, oil immersion). This objective focused the laser beam to produce the optical trap and also formed a bright-field image of trapped particles on a CCD camera. Laser power was 85–90 mW at the sample. The sample was mounted on a computer-controlled, custom-built *x-y-z* piezo translation stage. The 0.55 N.A. condenser of the microscope was used to collect forward-scattered laser light and to form a slightly de-focused image of the trap on a quadrant photodiode (model S4349, Hamamatsu, Middlesex, NJ). Voltage signals from the four quadrants were amplified and sent to a data acquisition board (AT-MIO-16E2, National Instruments, Austin, TX) in a 486–66 MHz computer where they were processed by custom-written Labview (National Instruments, Austin, TX) software to yield the x or y displacement of a trapped bead. In experiments where axial (z) displacements were measured, the de-focused image of the trap was centered on one element of the quadrant photodiode. This gave maximal sensitivity to axial displacements and minimal sensitivity to radial displacements (Ghislain et al., 1994). The same board and software used for data acquisition provided the analog signal for control of the piezo stage. Because most of the signals to be analyzed were from surface-bound beads, the quadrant detector sensitivity was determined by translating a bead affixed to a coverslip through the laser trap via the piezo stage and measuring the amplitude of the resulting signal. The detector sensitivity obtained in this manner was then used to estimate the uncertainty in position measurements due to instrument noise. From power spectra of detector signals obtained with an empty trap it was determined that the root-mean-square (rms) noise was 0.8 nm between 10 Hz and 10 kHz at the laser power used in typical experiments (see Fig. 3 *B*).

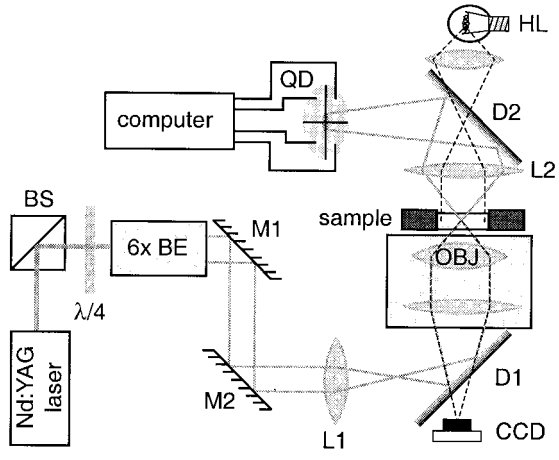

FIGURE 2 Diagram of the optical tweezers apparatus. Light (1064 nm) from a diode-pumped Nd:YAG laser is circularly polarized by passage through a polarizing beam splitter cube (BS) and a quarter-wave plate (λ/4). A 6× beam expander (6x BE) increases the diameter of the beam to ~1.5 cm. Mirrors 1 and 2 (M1 and M2) steer the expanded beam into the bottom camera port of the microscope. Lens 1 (L1) forms a real image of M2 at the back focal plane of the microscope objective (OBJ), allowing manual lateral translation of the trap's position in the sample via adjustment of the mirror's angle. Dichroics 1 and 2 (D1 and D2) separate the infrared trapping light from visible light of a tungsten-halogen lamp (HL) used to produce a bright-field image of the sample. This image is projected onto a CCD camera for viewing on a television monitor. Lens 2 (L2) is the condenser for the bright-field illumination system and also serves to focus the infrared light of the trap onto a quadrant detector (QD). Voltage signals from the four quadrants are amplified and sent to an analog-to-digital converter onboard a 486–66-MHz computer for processing and storage.

Calibration of optical trap

To convert displacement signals into forces, the stiffness of the optical trap in the radial direction had to be determined. This was done using the standard viscous drag calibration technique, whereby a lateral hydrodynamic drag force $F = -\gamma v$ was applied to a trapped bead by moving the surrounding fluid past it via periodic motion of the piezo stage. γ is the viscous drag coefficient and v is the velocity of the fluid with respect to the particle. Measurement of the resulting bead displacement allowed determination of a force-distance relationship. For comparison, the trap stiffness k_{trap} was also estimated from the corner frequency f_c of the displacement signal power spectrum using the relationship $k_{trap} = 2\pi\gamma f_c$ (Gittes and Schmidt, 1998). New viscous drag calibrations and power spectra were obtained every time a fresh sample was mounted on the microscope. Though the force-distance relationship for beads trapped very near the substrate deviated somewhat from linearity, as shown in Fig. 3 *A*, the spring constants obtained from linear fits to such data agreed very well with corner frequency measurements (see Fig. 3 *B* for an example).

When a bead is very close to a coverslip, the coefficient γ is sensitive to the bead-surface separation distance δ. Thus, it was important to have a reliable indicator of bead height during scanning and calibration, and the bead's axial position fluctuations proved to serve well in this capacity. It was found that when the z-piezo was used to gradually move the coverslip away from a trapped bead, there was an abrupt increase by a factor of ~2 in the rms amplitude of axial voltage signals as the bead-surface separation passed ~100 nm. (Because corner frequency measurements indicated that the axial spring constant increased with separation (up to ~3 μm), this increase in fluctuation amplitude was presumably due to an increase in detector sensitivity.) Successful scanning experiments were all characterized by the low-amplitude z-fluctuations; therefore, beads were positioned in the same height range for calibrations. To accomplish this, the piezo stage was used to translate the sample back and forth laterally. Simultaneously, the microscope focus knob was used to move a trapped bead down toward the substrate while monitoring the bead's axial position fluctuations. When the rms amplitude was the same as that observed during rupture force measurements (12 ± 2 nm), the viscous drag calibration was performed. If a bead formed bonds with the surface during the calibration, the focus knob was used to increase the separation slightly.

Because the binding sites were just out of reach of the trapped beads during calibrations, one can argue that the distance between the surface of the bead and surface of the coverslip was rarely smaller than $z_{max} \approx 24$ nm (see Appendix). If 95% of a bead's fluctuations are smaller than 2 × rms (also 24 nm), it is reasonable to expect that δ is at least 48 nm but less than 100 nm (as indicated by the axial signal rms). This range of values for δ implies that the ratio δ/a (where a is the bead radius) lies between 0.09 and 0.19 for 1.03-μm beads. Therefore, the expression below (known as the

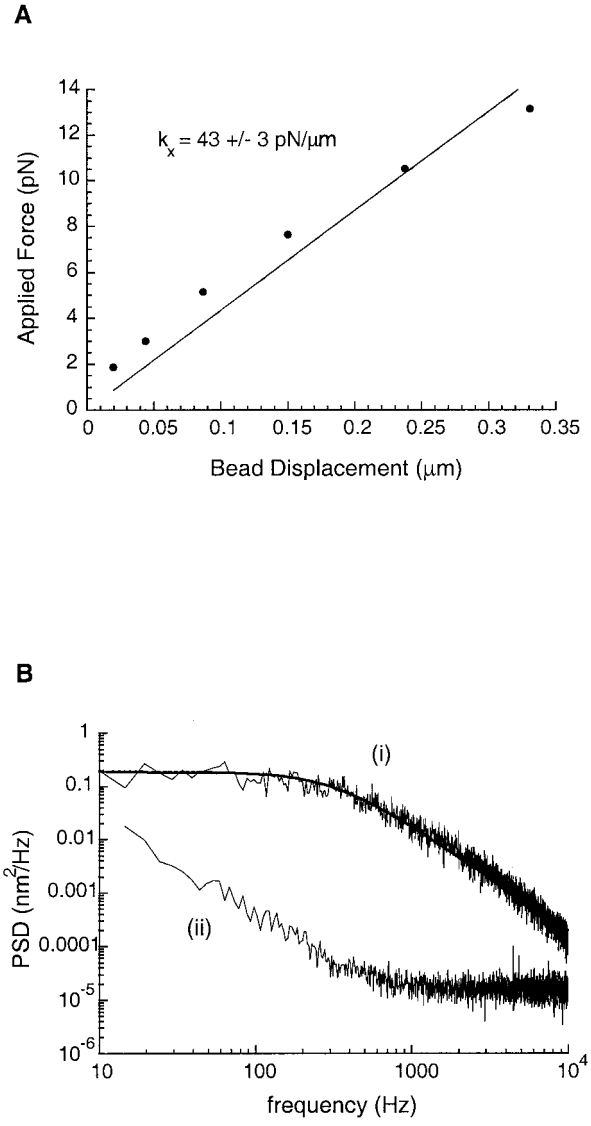

FIGURE 3 Characterization of optical tweezers. (*A*) Force-displacement relationship obtained during viscous drag calibration for a 1-μm polystyrene bead trapped near a glass coverslip (distance between bead surface and coverslip is on the order of 48 nm). ●, experimental data; ——, fit of the data to $F = k_x(x - x_0)$. Note that this fit is for comparison to *B* only. (*B*) Power spectral density of lateral displacements for a 1-μm polystyrene bead trapped ~48 nm from glass coverslip (*i*) and the empty optical trap (*ii*). The thicker solid line through (*i*) is from a least-squares fit of the data to a Lorentzian function. The corner frequency from this fit implies a spring constant k_x of 44 ± 2 pN/μm.

Faxen correction) may be used to calculate the viscous drag coefficient γ for a sphere moving through a stationary fluid of viscosity η (Happel and Brenner, 1973):

$$\frac{\gamma}{\gamma_0} = \frac{\gamma}{6\pi\eta a} \sim \frac{1}{\left(1 - \frac{9}{16}\left(\frac{a}{a+\delta} + \frac{1}{8}\frac{a}{a+\delta}\right)^3\right)} \quad (2)$$

The range of δ/a values given above implies that $\gamma/\gamma_0 = 1.69 \pm 0.03$.

Rupture force measurement

The rupture force for each detected binding event was calculated from the maximum lateral displacement of the bead away from the trap center just before bond breakage. In these experiments, F_T, the force applied by the optical trap to a substrate-bound bead, is taken to be tangential to the surface and in the *x*-direction. Tangential frictional forces between bead and surface are assumed to be negligible based on the observed lack of adhesion between uncoated beads and uncoated surfaces. The force of the intermolecular bond, F_B, acts along a tether joining the bead to the surface, and forms an angle θ between the tether and the surface normal (see Fig. 4 *A*). If a bound bead rotates around its tether during a scan and subsequently contacts the surface, a repulsive force normal to the surface, F_N, is also applied to the bead. (The force F_N will actually have two contributions: one from contact with the surface and one due to axial displacement of the bead away from the optical trap's center. These two forces will act in the same direction, however, and so have been combined into a single force vector, F_N.) This normal force will enhance the effect of F_T by a geometric factor that depends on $\sin\theta$ as shown in Fig. 4 *A*. The movement of the surrounding fluid past the bound bead will also lead to a hydrodynamic drag force not shown in Fig. 4 *A*. However, the scan velocities used in these experiments ranged from 1.0 to 18 μm/s; estimates of the resulting drag force suggest that it was, at most, one to two orders of magnitude smaller than the force applied by the optical tweezers at rupture. Consequently, hydrodynamic drag forces were neglected.

Because the angle θ is a function of the unknown length of the surface-bead tether as well as of the bead radius, it was necessary to estimate it from detailed examination of individual event traces such as those in Fig. 5. The time at which the average position of the bead began to drift away from the center of the trap provided an indication of the time of bond formation; the approximate position of the binding site (point B in Figs. 4 *A* and 5 *A*) on the sample could then be determined from the stage-driving signal. The time at which the bead became pinned to the substrate was marked by a noticeable drop in the amplitude of position fluctuations, which allowed determination of the point of contact (point C in Figs. 4 *A* and 5 *A*). The distance *D* in Fig. 4 *A* was taken to be the distance traveled by the stage between these two points, X_S. Once a value of *D* was found, θ (and tether length *L* if desired) could be calculated. As not all traces could be used to determine the angle in this manner, average values for X_S were obtained for each similar data set and used to calculate an enhancement factor. Although the fractional uncertainty in each measurement of *D* was on the order of 20–25% (compared with the 2.3% uncertainty in bead radius reported by the manufacturer), measurements from multiple IgG-SpA events were distributed about a single mean with a standard error of 7% (see Fig. 4 *B*).

Using the stage displacement X_S as a measure of the distance *D* is equivalent to assuming that the line connecting points B and C is parallel to the scan direction. If this is not the case, the above procedure will lead to an underestimate of the distance *D* and to a value of θ that is too small (see Fig. 4 *C*). To estimate the magnitude of this error, one can assume that potential binding sites on the substrate must lie within a circle of radius $r \approx 3s$ around the trap center, where $s = 9$ nm is the rms radial displacement of a trapped bead. For a typical value of 100 nm for X_S (for 1-μm beads), if point B is 27 nm away from the scan line, the ratio of the observed X_S to the unknown *D* will be

$$\frac{X_S}{D} = \cos\left(\arctan\left(\frac{27}{100}\right)\right) = 0.965. \quad (3)$$

Thus, any error in the enhancement factor introduced by assuming that the three force vectors lie in a single plane is on the order of 3%. The final fractional uncertainty in an individual force measurement, combining the uncertainty in F_T (due to uncertainties in γ, the quadrant detector, the piezo stage, and parameters determined from trap calibrations) with the uncertainties in the enhancement factor described above is ~25%.

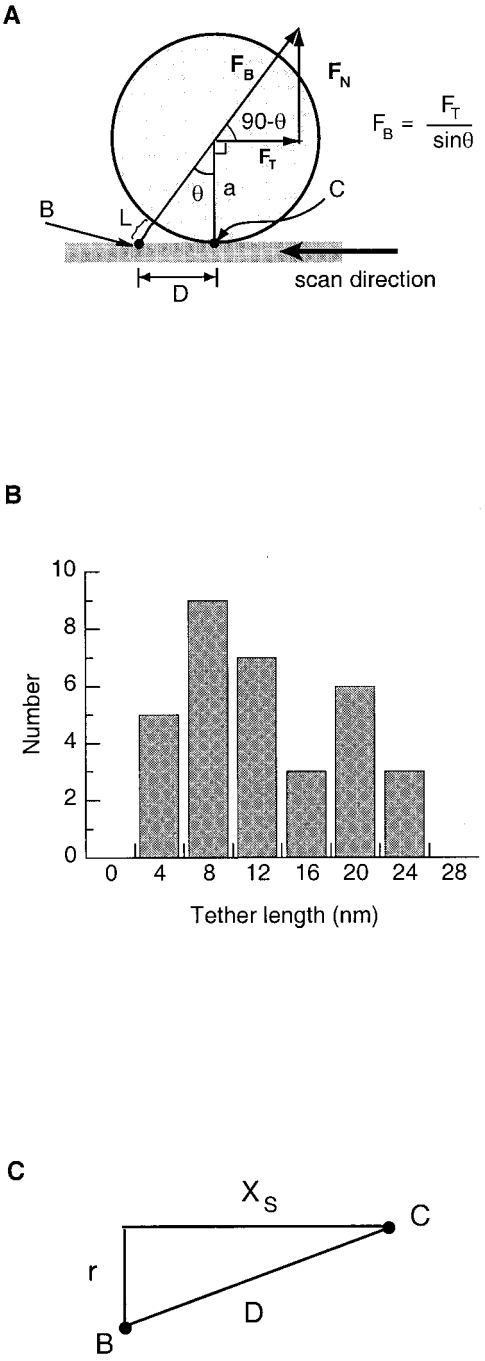

FIGURE 4 (*A*) Geometry of force enhancement during rupture force experiments. The force applied to rupture the bead-surface bond is a vector sum of the tangentially applied trap force F_T and a normal force F_N resulting from contact and axial displacement of the bead. The enhancement factor is equal to $1/\sin\theta$, as shown. Neither the tether length L nor the angle θ can be measured directly; rather, θ must be calculated from a, the known bead radius, and D, the distance between the tether point B and the contact point C. (*B*) Histogram of tether lengths obtained from binding-rupture events observed on SpA substrates with IgG-beads as described in Materials and Methods. (*C*) View from above the sample showing the relationship between D and X_S, the distance traveled by the sample between binding and bead contact for a case where the scan direction is not parallel to the line connecting points B and C. r is the distance between the binding site and the scan line (see text for details on estimating r).

RESULTS

Experimental technique

Bond detection

Binding events were detected by holding an IgG-coated bead above the substrate with the optical trap while scanning the substrate sample back and forth along a line perpendicular to the optical axis and monitoring the bead's position. These events were characterized by the distinctive displacement signals seen in Fig. 5, *A* and *B*. In early trials, it was found that using an IgG:bead ratio of 5 or less during the coating procedure resulted in only a small fraction (less than 20%) of the beads showing binding events on SpA substrates. For final rupture force experiments, an IgG:bead ratio of 10 was chosen for bead preparation, as 65–70% of these displayed binding events on SpA surfaces. Even a bead with 10 molecules attached should have at most a 9% chance that an observed event could be due to more than one IgG-protein bond (see Appendix). Indeed, a small number of rupture events that were characterized by position data suggestive of two bonds, such as that in Fig. 5 *B*, were observed. These two-bond events were not included in later force analyses.

Specific versus nonspecific interactions

At the salt concentration used in these experiments (0.15 M NaCl), colloidal particles will adhere strongly to a bare glass surface due to a combination of interactions that has been modeled by the Derjaguin–Landau–Verwey–Overbeek theory (Israelachvili, 1992). A fairly low concentration (0.08 mg/ml) of κ-casein in the experimental buffer largely alleviated the strong nonspecific interactions between beads and coverslips. The mechanism by which this is accomplished is not entirely clear; it is likely, however, that the reduction in nonspecific adhesion is due to a combination of steric, electrostatic, and other effects (Israelachvili, 1992). At concentrations near that used here, casein will form a 10-nm-thick layer on solid surfaces. It has been shown that such casein-coated surfaces exhibit a very weak attraction for each other, requiring only ~1.5 pN of force to separate them (Chowdhury and Luckham, 1995). However, casein did not entirely prevent nonspecific rupture events that required significantly more than 1.5 pN of applied force.

To characterize the density and distribution of nonspecific events, control experiments were performed on three types of control samples using G-IgG-coated beads (2.6-μm-diameter polystyrene) in PBS with 0.08 mg/ml casein. These results are summarized in Fig. 6, which depicts the line density of rupture events as a function of force. Substrates exposed to 0.1 M ethanolamine (which reacts with the amine-reactive cross-linker GMBS) in place of SpA showed the lowest number of binding events, whereas BSA-coated substrates showed slightly more. In both of these

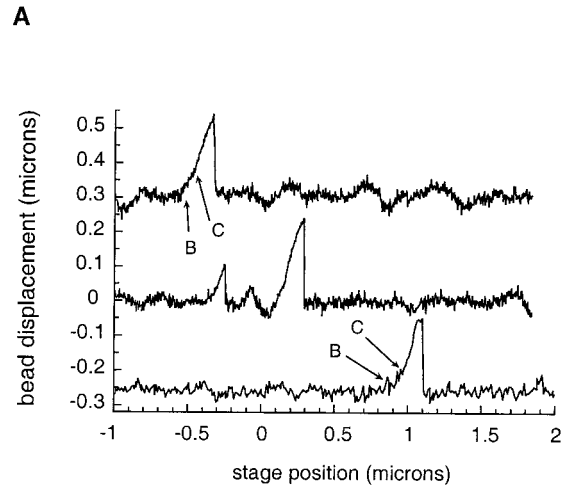

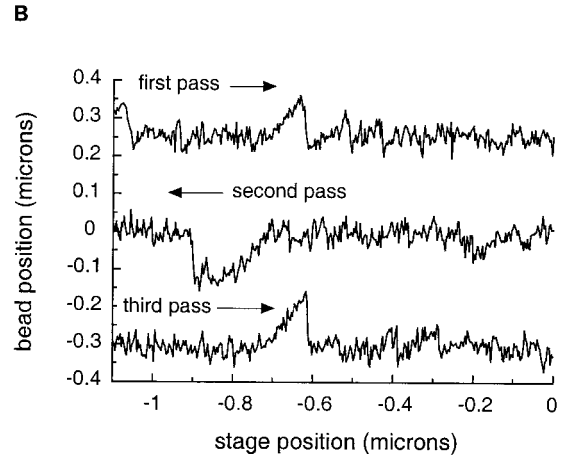

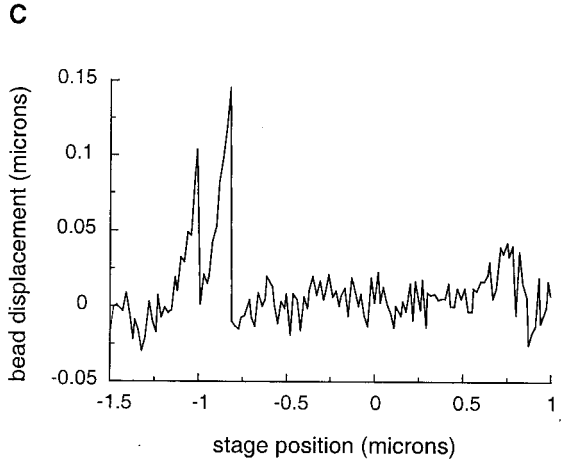

FIGURE 5 (*A*) Examples of individual binding-rupture events observed on SpA substrates with 1-μm polystyrene M-IgG beads (substrate is moving from left to right in all three traces). Bead displacements were obtained from quadrant detector signals; stage position was known from the response of the piezoelectric scanning stage. In two of the traces, tether point B and contact point C (as described in the text and in Fig. 4 *A*) are labeled. (*B*) An example of repeated binding events at the same location on the substrate observed with G-IgG on 2.6-μm polystyrene beads. (*C*) Possible two-bond event observed with B-IgG on 1-μm polystyrene beads.

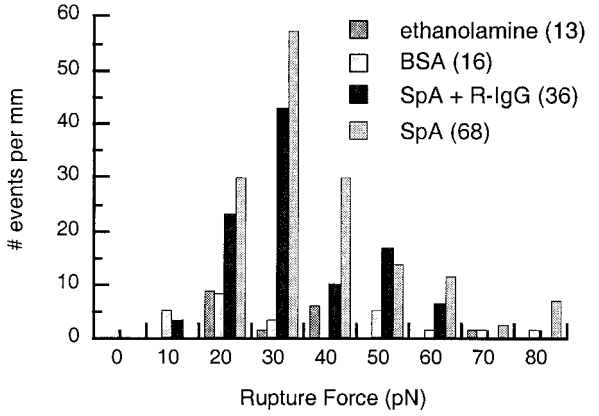

FIGURE 6 Comparison of linear bond densities for control substrates and SpA substrates. All data were acquired using 2.6-μm polystyrene beads coated with G-IgG. Plotted are rupture force histograms normalized by the total distance scanned on a particular substrate. The total number of events observed on each substrate is given in parentheses in the figure legend.

treatments, the median rupture force was ~30 pN, lower than that for SpA-coated substrates.

A third control experiment was performed using G-IgG beads and SpA coverslips, in a buffer containing 0.1 mg/ml R-IgG in addition to the casein. The R-IgG was intended to block the G-IgG-SpA interaction; however, this sample showed significantly more binding events than the two other controls (though still fewer than an SpA sample without R-IgG in solution). This may be because the concentration of R-IgG was too low to effectively block all SpA sites on the surface. Additionally, some R-IgG might have tightly adsorbed to the beads out of solution during the experiment. In this case, some of the binding events detected may have been between bead-adsorbed R-IgG and SpA. Still another possibility is that the R-IgG did block the SpA binding sites, but there was a nonspecific interaction between it and G-IgG on the beads.

A related concern in these experiments is the possibility that some or all of the events observed are due to breakage of either an SpA-surface bond or an IgG-bead bond. The cross-linkers used in the coating procedures form covalent linkages between proteins and substrates that should be too strong to sever with the applied forces here. A typical covalent bond requires 5–10 nN to break it (Israelachvili, 1992), a force that is well over 20 times the maximum force applied by the optical tweezers after leverage enhancement (see below). The durability of these attachments is confirmed by frequent occasions when binding-rupture events occurred two or more times at the same location during

multiple scans over a line, indicating that SpA molecules were not being removed from the surface (see Fig. 5 *C* for an example). In addition, beads were stored in a buffer containing 0.01% detergent and then washed in detergent-free buffer immediately before use. Such treatment should remove any noncovalently adhered IgG molecules that might be present on the beads.

Leverage

Initial examination of the displacement signals obtained during binding events suggested that bead-surface contact was occurring before bond rupture. Brownian motion of the bound beads was suppressed considerably in virtually every event recorded, suggesting that the beads were pinned firmly to the substrate. Closer analysis of individual events such as those of Fig. 5 *A* shows some Brownian motion during the initial movement of the bead away from the trap center that was damped by the time bond rupture took place. This behavior suggests that after bond formation, a bound bead would pivot about its connection point as it moved away from the trap center until the bead made contact with the surface. This bead-surface contact resulted in an enhancement of the applied force due to leverage. To calculate the degree of enhancement, one needs to know the length of the tether that connects the bead to the substrate. Using the procedure described in Materials and Methods it was determined that the mean tether length L was 10 nm (SE = 1 nm) for SpA samples and 1.0-μm IgG-beads, implying a force enhancement factor of 5.3 $\pm$ 0.8.

Further evidence for leverage was obtained by changing the diameter of the beads. Experiments on identically prepared SpA substrates were performed using polystyrene beads coated with an average of 10 G-IgGs per bead and having diameters of either 1.0 or 2.6 μm. The uncorrected rupture force histograms were of similar widths in the two experiments but were centered about different means. In the case of 2.6-μm beads, the mean trap force at rupture was 2.8 pN, whereas with 1.0-μm beads, it was 6.1 pN. Subsequent measurements of tether lengths and correction of the forces shifted the means to 34 pN for the former and 32 pN for the latter (data not shown).

An additional test would be to conduct these experiments using an axial approach-retract scan at the location of an IgG-SpA bond, as is done routinely using the atomic force microscope. In this case the force applied by the optical trap would be parallel to the tether rather than at an angle to it, but the force required to sever the bond should be the same. Implementation of such a design would require an optical trap with a stronger axial gradient than the instrument used here could produce, as forces higher than 100 pN are needed to obtain rupture force histograms. (The maximum axial force that could be applied by this optical trap was ~20 pN for 1-μm latex spheres.) Several attempts were made to perform axial approach-retract scans at single points on the coverslip, resulting in two types of observed behavior. Either there was no hysteresis in the position data that would indicate binding and rupture, or there was binding too tight to be disturbed by the optical trap. Though not quantitative, these observations are, at least, consistent with the range of forces measured in the tangential-scan experiments.

Survival probabilities

It has been well established through equilibrium binding experiments that SpA binds to IgG with an affinity that is species dependent. Published figures for the K_D of the SpA-IgG interaction are summarized in Table 1. Kuo and Lauffenberger (1993) demonstrated a logarithmic relationship between dissociation constant and the shear force required to detach IgG-coated beads from SpA-coated surfaces. Because extrapolation of their data down to single pairs of molecules yielded results for detachment forces in the range accessible to the optical tweezers (see Table 1), one would expect to observe a similar correlation among individual SpA-IgG bonds. Experiments were performed with four species of IgG: goat, rabbit, mouse, and bovine. Fig. 7 displays the force-dependent survival probability, obtained from rupture force histograms for each type of IgG. The median rupture forces for the four types of IgG-

TABLE 1 Dissociation constants, bond energies, and measured rupture forces for SpA interactions with several species of IgG molecules

	K_D (M)*	E_b (eV)†	F_R (pN)‡	$F_{0.5}$ (pN)§(SD)	Number of events
Rabbit IgG	1.1×10^{-8}	0.46	80 $\pm$ 10	44 (41)	36
Mouse IgG	1.9×10^{-7}	0.39	20 $\pm$ 5	35 (30)	48
Bovine IgG	1.2×10^{-7}	0.40	NA	35 (28)	74
Goat IgG	4×10^{-6}	0.31	5 $\pm$ 10	25 (25)	83

*K_D figures are from Langone (1982; rabbit IgG) and Moks *et al*. (1986; mouse, bovine, and goat IgG).
†Estimated from $\Delta G_D = -k_B T \ln K_D$, using $k_B T = 0.025$ eV.
‡Adhesion strength per receptor as determined by Kuo and Lauffenburger (1993) through extrapolation of data from radial flow detachment assays down to single bonds. NA, no data on this species of IgG was available.
§Optical tweezers measurements of median rupture force for the observed bonds between IgG-coated 1.0-μm polystyrene beads and SpA-coated surfaces in phosphate-buffered saline at pH 7.4.

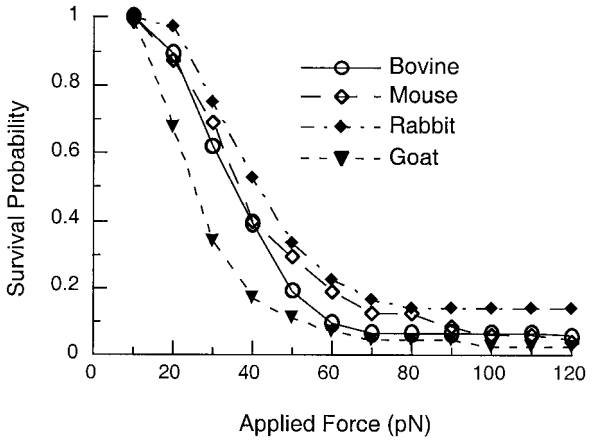

FIGURE 7 Force-dependent bond survival probabilities for four species of IgG beads on identical SpA-coated coverslips, obtained from rupture force histograms. The median rupture force, $F_{0.5}$, is taken to be the applied force at which 50% of the bonds were ruptured.

SpA bond are listed in Table 1, along with the results of Kuo and Lauffenburger (1993) for comparison. These results are in general agreement with theirs, with G-IgG showing the lowest median rupture force (25 ± 3 pN) and R-IgG showing the highest (44 ± 12 pN).

DISCUSSION

The technique

The optical tweezers are a highly sensitive and versatile force transducer in a variety of applications. From these results, it is clear that a scanning optical tweezers can be used to locate and characterize individual protein-protein bonds and that leverage provided by the probe itself can be used to expand the range of accessible forces. Because the probe in these experiments is able to undergo axial Brownian motion as the sample is scanned beneath it, it can be considered to be operating in a thermally driven tapping mode, akin to the mode of atomic force microscopy of the same name (Martin et al., 1987). This method of sampling the surface has a distinct advantage in that it provides many opportunities for a molecule on the bead to encounter a binding site on the surface, yet it minimizes the likelihood of nonspecific interactions by maintaining an ~50-nm separation between bead and surface. One way to further prevent the occurrence of such events might be to compromise some of the leverage gained during contact by including a long polymeric linker between ligand and bead. This should allow one to maintain a somewhat larger distance between bead and surface during scanning while still giving some amplification (a factor of 2 or 3) of the trap force during binding-rupture events.

Even with the probe-surface separation of ~50 nm, binding due to nonspecific interactions was not completely eliminated under conditions employed in these experiments. However, the rupture force histograms from control experiments shown in Fig. 6 suggest that the overall number of nonspecific interactions that occurred between IgG probes and SpA substrates was small compared with the number of specific bonds formed. If one assumes that the BSA substrates allow the same number of nonspecific interactions as SpA substrates, one can estimate the probability that a bond observed while probing an SpA substrate with an IgG-coated bead is, in fact, a nonspecific bond. According to Fig. 6, scanning 1 mm of a BSA-coated surface with a G-IgG bead should give ~16 rupture events; scanning 1 mm of an SpA-coated surface with an identical bead should give ~155 events. Thus, there is roughly a 17% chance that an event classified as IgG-SpA is instead a nonspecific interaction. In theory, it should be possible to use a similar argument to correct the SpA rupture force histograms. However, to do so, one must make a stronger assumption than in the previous argument: that the distribution of rupture forces observed with the BSA sample is an accurate representation of the distribution of nonspecific rupture forces that occur on an SpA sample. As only one set of control experiments was performed, it is unclear at this time whether or not such an assumption is valid. In the future it will be interesting to refine this experimental design and take this approach even further, using it to identify and characterize multiple populations of specific protein-protein interactions on a single substrate.

Using probe-surface contact to extend the range of forces accessible to the optical tweezers does introduce some difficulties in force measurement not found in experiments using a trapped probe far from any flat surface. In the arrangement presented here, a surface-bound, trapped bead is able to pivot around its linkage point as the surface moves. This pivoting will pull the bead down toward the surface, causing both radial and axial displacements of the bead away from equilibrium. Because trap calibrations involved only radial displacements of unattached beads, it is possible that the effective radial trap stiffness during rupture force experiments differed somewhat from that determined during calibration. This effect should be quite small for axial displacements on the order of 50 nm, however. Verification requires a complete theoretical analysis of the axial dependence of radial trapping force in the intermediate regime where $\lambda \approx a$ (a = bead radius) and where the laser beam is highly focused. Published analyses of trapping forces for this situation (Wohland et al., 1996; Visscher and Brakenhoff, 1992) have so far been confined to calculating the dependence of the radial force component on radial displacements of the particle. It is likely, however, that the relative magnitude of the effect in the intermediate regime is comparable to that in the ray optics regime ($\lambda \gg a$) for which a full theoretical treatment has been carried out (Ashkin, 1992). These theoretical results indicate that for a bead of radius a in the ray optics regime, an axial displacement of the focal region by a distance on the order of $0.1a$

will result in a very small (<5%) decrease in the radial restoring force experienced by the bead. This suggests that at worst, the rupture forces measured for the four IgG-SpA interactions are systematically high by an amount that is small relative to the overall uncertainty. The observed differences in median rupture force between the different species of IgG would not be affected by this systematic error, however.

The interpretation of experimental data relies on construction of an accurate picture of all forces and torques acting on a bead at the time of bond rupture. In particular, hydrodynamic forces and surface forces must be accounted for in any rigorous analysis. Employing slow scan speeds should minimize the impact of neglecting the former. Miscellaneous surface forces such as van der Waals contacts are more difficult to eliminate from the picture; however, the presence of casein in the buffer eliminated virtually all adhesion between probes and surfaces (in the absence of SpA and IgG), suggesting that such forces do not play a significant role in the binding-rupture events attributed to specific bonds.

Comparison with previous rupture force measurements

A simple estimate of the single-bond energies E_b based on the equilibrium free energies of dissociation shown in Table 1 suggests that the force required to rupture a R-IgG-SpA bond should be greater than that required to rupture a G-IgG-SpA bond by a factor of 1.5 (assuming the same bond length for both), despite the ~400-fold difference in affinities. Experimental results presented here agree with this prediction: the median force required to rupture a R-IgG-SpA bond was found to be ~1.8 times greater than that for G-IgG.

The forces required to disrupt several intermolecular interactions have been probed by a number of investigators using various techniques. Experiments using the atomic force microscope have shown that the streptavidin-avidin interaction requires an applied force of 160 pN for rupture (Florin et al., 1994). In similar experiments, Hinterdorfer et al. (1996) found the force required to disrupt an antibody-antigen interaction was near 250 pN. Both of these interactions are considered highly specific and irreversible, with K_D values around 10^{-9} M and dissociation rates (in the absence of applied force) on the order of 10^{-3} s^{-1} (Ito and Kurosawa, 1993). In contrast, the protein A-IgG interaction varies in specificity from a K_D of 10^{-9}-10^{-8} M for rabbit IgG to 10^{-6} M for sheep or goat IgG (Lindmark et al., 1983; Langone, 1982). Protein A therefore provides an opportunity to explore the effect of applied mechanical force on similar interactions of varying affinity. The SpA-IgG pair does have one notable disadvantage, which is that SpA has been shown to have both a high-affinity IgG-binding site on the F_c portion as well as a lower-affinity site on the F_{ab} fragment (Moks et al., 1986; Sandor and Langone, 1982). It might be possible, however, to study each type of interaction separately if one were to use more sophisticated cross-linking protocols to control the orientations of the immobilized proteins.

In this study, applied force was ramped continuously from zero up to the rupture force by slowly moving a bound bead away from the center of the optical trap. A more rigorous analysis of the observed survival probability curves must therefore take into account the loading rate. This issue has been explored by Evans and Ritchie (1997) in Brownian dynamics simulations and by Izrailev et al. (1997) in molecular dynamics simulations of forced unbinding. Both of these groups predicted that the median force required to rupture an intermolecular bond should increase logarithmically with loading rate. A recent experimental work (Simson et al., 1999) confirmed that the interaction between SpA and rabbit IgG does indeed behave in such a manner, with a rupture force that increases rapidly with loading rate as it is increased to ~100 pN/s. Continued ramping of loading rate beyond this value leads to a much less dramatic increase in rupture force, consistent with the logarithmic dependence.

The optical tweezers experiments presented here, however, failed to show any clear dependence of median rupture force on scan velocity (data not shown). A likely explanation for this is that even the slowest scan rates employed gave high loading rates due to the leverage effect. Assuming that a tethered bead was in contact with the substrate for the majority of the load duration, one can calculate the loading rate for each rupture event using the trap's force-distance relationship, the scan rate, and leverage enhancement factor. Such calculations reveal loading rates ranging from 400 to 5300 pN/s, much higher than those employed by Simson et al. (1999). It will be of interest in the future to extend the range of scan speeds to much lower values than used here to explore the effect of loading rate on a variety of intermolecular interactions.

APPENDIX

To estimate the probability that an observed rupture event is due to more than one bond, we must first determine the fraction of a bead's surface area that falls within some threshold distance for bond formation when the bead is near a surface. When an IgG-coated bead is held with its bottom a distance δ away from an SpA-coated substrate, only a small portion of the bead's surface will be close enough to permit an interaction. Let z_{max} denote the maximum vertical distance between a point on the bead and a point on the substrate that will allow bond formation. Because δ fluctuates due to Brownian motion of the bead, the area falling within z_{max} fluctuates as well. It is of interest to determine the maximum value of this contact area, for this will allow us to put an upper limit on p, the probability that any one IgG sits within the interaction range. As seen in Fig. 8, the contact area is maximum when the bead touches the surface ($\delta = 0$). Neglecting any deformation of the sphere, we can see that the maximum contact area is given by the following integral:

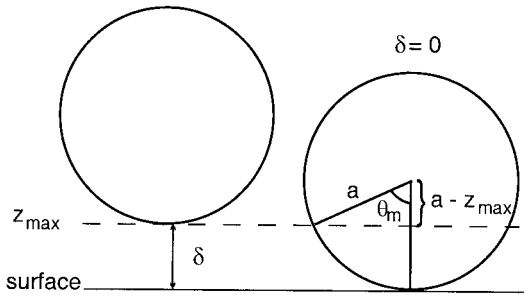

FIGURE 8 Illustration of geometry used to estimate maximum possible bond formation area for a spherical bead of radius a near a planar surface. δ is the minimum distance between the surface of the bead and the nearby planar surface. z_{max} is the maximum allowed distance between interacting sites on the bead surface and planar surface.

$$\text{maximum contact area} = 2\pi a^2 \int_{\theta_m}^{\pi} \sin\theta \mathrm{d}\theta, \qquad (4)$$

where

$$\theta_m = \pi - \cos^{-1}\left(\frac{a - z_{\max}}{a}\right). \qquad (5)$$

This reduces to the following simple relationship:

$$\text{maximum contact area} = 2\pi a z_{\max} \qquad (6)$$

A reasonable estimate for z_{max} is ~18–30 nm, allowing ~8–10 nm for the average diameter of an SpA (Langone, 1982) and ~10–20 nm for the average length of an IgG (Cozens-Roberts et al., 1990). This yields a value for the maximum contact area that is ~2–3% of the total sphere area.

The probability that n IgG molecules will fall inside the maximum contact area is

$$P_n = \frac{N!}{n!(N-n)!} p^n (1-p)^{N-n}, \qquad (7)$$

where N = the total number of IgG molecules on a bead (10 for an average bead) and p = (contact area)/(total area) = 0.02–0.03. The probability that the actual number of SpA-IgG bonds (x) involved in a particular event is exactly one is given by the following conditional probability:

$$P(x = 1 | x > 0) = \frac{P_1}{1 - P_0} \qquad (8)$$

Values of N and p for conditions used imply a value of 0.87–0.91 for this conditional probability, suggesting that rupture events due to two or more bonds are expected to be rare.

I express my gratitude to Dr. Watt W. Webb for his generous support of this work, carried out at the Developmental Resource for Biophysical Imaging and Opto-electronics at Cornell University, Ithaca, NY. In addition, thanks go to Neil Switz for help in construction of the instrument and quadrant detector amplifier, Dr. Jerome Mertz for advice concerning instrumentation, and Dr. Philip Everson at Swarthmore College for assistance with statistical analyses. Finally, I thank the anonymous reviewers for helpful comments and criticisms.

This project was supported by National Institutes of Health P41–2RR04224 and NSF BIR-9419978.

REFERENCES

Alon, R., D. A. Hammer, and T. A. Springer. 1995. Lifetime of the P-selectin-carbohydrate bond and its response to tensile force in hydrodynamic flow. *Nature.* 374:539–542.

Ashkin, A. 1992. Forces of a single-beam gradient laser trap on a dielectric sphere in the ray optics regime. *Biophys. J.* 61:569–82.

Bhatia, S. K., L. C. Shriver-Lake, K. J. Prior, J. H. Georger, J. M. Calvert, R. Bredehorst, and F. S. Ligler. 1989. Use of thiol-terminal silanes and heterobifunctional crosslinkers for immobilization of antibodies. *Anal. Biochem.* 178:408–413.

Chang, K. C., and D. A. Hammer. 1996. Influence of direction and type of applied force on the detachment of macromolecularly-bound particles from surfaces. *Langmuir.* 12:2271–1282.

Chowdhury, P. B., and P. F. Luckham. 1995. Interaction forces between κ-casein adsorbed on mica. *Colloids Surfaces B.* 4:327–334.

Cozens-Roberts, C., J. A. Quinn, and D. A. Lauffenburger. 1990. Receptor-mediated adhesion phenomena: model studies with the radial-flow detachment assay. *Biophys. J.* 58:107–125.

Evans, E., D. Berk, and A. Leung. 1991. Detachment of agglutinin-bonded red blood cells. I. Forces to rupture molecular-point attachments. *Biophys. J.* 59:838–848.

Evans, E., and K. Ritchie. 1997. Dynamic strength of molecular adhesion bonds. *Biophys. J.* 72:1541–1555.

Finer, J. T., R. M. Simmons, and J. A. Spudich. 1994. Single myosin molecule mechanics: piconewton forces and nanometer steps. *Nature.* 368:113–118.

Florin, E-L., V. T. Moy, and H. E. Gaub. 1994. Adhesion forces between individual ligand-receptor pairs. *Science.* 264:415–417.

Ghislain, L. P., N. A. Switz, and W. W. Webb. 1994. Measurement of small forces using an optical trap. *Rev. Sci. Instrum.* 65: 2762–2768.

Gittes, F., and Schmidt, G. F. 1998. Signals and noise in micromechanical measurements. *Methods Cell Biol.* 55:129–156.

Happel, J., and H. Brenner. 1973. Low Reynolds number hydrodynamics with special applications to particulate media, 2nd ed. Noordhoff International Publishing, Leyden, The Netherlands.

Helmerson, K., R. Kishore, W. D. Phillips, and H. H. Weetall. 1997. Optical tweezers-based immunosensor detects femtomolar concentrations of antigens. *Clin. Chem.* 43:379–383.

Hinterdorfer, P., W. Baumgartner, H. J. Gruber, K. Schilcher, and H. Schindler. 1996. Detection and localization of individual antibody-antigen recognition events by atomic force microscopy. *Proc. Natl. Acad. Sci. U.S.A.* 93:3477–3481.

Israelachvili, J. N. 1992. Intermolecular and Surface Forces. Academic Press, San Diego, CA.

Ito, W., and Y. Kurosawa. 1993. Development of an artificial antibody system with multiple valency using an Fv fragment fused to a fragment of protein A. *J. Biol. Chem.* 268:20668–20675.

Izrailev, S., S. Stephaniants, M. Balsera, Y. Oono, and K. Schulten. 1997. Molecular dynamics study of unbinding of the avidin-biotin complex. *Biophys. J.* 72:1568–1581.

Kuo, S. C., and Lauffenburger, D. A. 1993. Relationship between receptor/ligand binding affinity and adhesion strength. *Biophys. J.* 65:2191–2002.

Langone, J. J. 1982. Protein A of *Staphylococcus aureus* and related immunoglobulin receptors produced by streptococci and pneumococci. *Adv. Immunol.* 32:158–252.

Lindmark, R., K. Thorén-Tolling, and J. Sjöquist. 1983. Binding of immunoglobulins to protein A and immunglobulin levels in mammalian sera. *J. Immunol. Methods.* 62:1–13.

Martin, Y., C. C. Williams, and H. K. Wickramasinghe. 1987. Atomic force microscope-force mapping and profiling on a sub-100-Å scale. *J. Appl. Phys.* 61:4723–4729.

Moks, T., L. Abrahamsén, B. Nilsson, U. Hellman, J. Sjöquist, and M. Uhlén. 1986. Staphylococcal protein A consists of five IgG-binding domains. *Eur. J. Biochem.* 156:637–643.

Nishizaka, T., H. Miyata, H. Yoshikawa, S. Ishiwata, and K. Kinosita. 1995. Unbinding force of a single motor molecule of muscle measured using optical tweezers. *Nature.* 377:251–254.

Pierres, A., A-M. Benoliel, and P. Bongrand. 1995. Measuring the lifetime of bonds made between surface-linked molecules. *J. Biol. Chem.* 270: 26586–26592.

Ros, R., F. Schweisinger, D. Anselmetti, M. Kubon, R. Schäfer, A. Plückthun, and L. Tiefenauer. 1998. Antigen binding forces of individually addressed single-chain Fv antibody molecules. *Proc. Natl. Acad. Sci. U.S.A.* 95:7402–7405.

Sagvolden, G. 1999. Protein adhesion force dynamics and single adhesion events. *Biophys. J.* 77:526–532.

Sandor, M., and J. J. Langone. 1982. Demonstration of high and low affinity complexes between protein A and rabbit immunoglobulin G antibodies depending on hapten density. *Biochem. Biophys. Res. Commun.* 106:761–767.

Simson, D. A., M. Strigl, M. Hohenadl, and R. Merkel. 1999. Statistical breakage of single protein A-IgG bonds reveals crossover from spontaneous to force-induced bond dissociation. *Phys. Rev. Lett.* 83:652–655.

Stout, A. L., and W. W. Webb. 1998. Optical force microscopy. *Methods Cell Biol.* 55:99–116.

Svoboda, K., C. F. Schmidt, B. J. Schnapp, and S. M. Block. 1993. Direct observation of kinesin stepping by optical trapping interferometry. *Nature.* 365:721–727.

Visscher, K., and G. J. Brakenhoff. 1992. Theoretical study of optically induced forces on spherical particles in a single beam trap. II. Mie scatterers. *Optik.* 90:57–60.

Voet, D., J. G. Voet, and C. W. Pratt. 1999. Fundamentals of Biochemistry. John Wiley and Sons, New York, NY.

Wohland, T., A. Rosin, and E. H. K. Stelzer. 1996. Theoretical determination of the influence of the polarization on forces exerted by optical tweezers. *Optik.* 102:181–190.

Yin, H., M. D. Wang, K. Svoboda, R. Landick, S. M. Block, and J. Gelles. 1995. Transcription against an applied force. *Science.* 270:1653–1657.